Letter

Multimessenger study of the Galactic diffuse emission with LHAASO and IceCube observations

Chengyu Shao,[1] Sujie Lin,[1,*] and Lili Yang[1,2,†]

[1]*School of Physics and Astronomy, Sun Yat-Sen University, No. 2 Daxue Road, 519082, Zhuhai China*
[2]*Centre for Astro-Particle Physics, University of Johannesburg, P.O. Box 524, Auckland Park 2006, South Africa*

(Received 9 July 2023; accepted 8 September 2023; published 29 September 2023)

With the breakthrough in PeV gamma-ray astronomy brought about by the LHAASO experiment, the high-energy sky is becoming richer. Recently, the LHAASO Collaboration reported the observation of a gamma-ray diffuse emission with energy up to the PeV level from both the inner and outer Galactic plane. In these spectra, there is a bump that is hard to explain using the conventional cosmic-ray transport scenarios. Therefore, we introduce two extra components corresponding to unresolved sources with exponential-cutoff-power-law (ECPL) spectral shape—one with an index of 2.4 and cutoff energy of 20 TeV, and another with an index of 2.3 and cutoff energy of 2 PeV. With our constructed model, we simulate the Galactic diffuse neutrino flux and find that our results are in full agreement with the latest IceCube Galactic plane search. We estimate the Galactic neutrino contributes ∼9% of astrophysical neutrinos at 20 TeV. In the high-energy regime, as expected, most of the neutrinos observed by IceCube should be from extragalactic environments.

DOI: 10.1103/PhysRevD.108.L061305

I. INTRODUCTION

The origin of cosmic rays (CRs) is one of the key questions in astrophysics. The CR energy spectrum includes knee and ankle features. It is generally believed that CRs with energies below the spectral knee at $\sim 10^{15}$ eV mainly come from our Galaxy, so-called Galactic cosmic rays (GCRs). While those with energies above the spectral ankle at $\sim 10^{18}$ eV are mostly from extragalactic energetic sources. Most CR particles lose their directional information due to the deflection and interaction with extragalactic and Galactic magnetic fields and mediums during their propagation. This additional uncertainty means that the origin of CRs near the knee remains unknown.

To resolve these issues, alternative methods have been adopted. Collisions between energetic CRs and ambient and interstellar mediums generate neutral (π^0) and charged pions ($\pi^{\pm}$), which decay to gamma rays and neutrinos. These secondary products detected on Earth will encode details of both the CR and target populations. The accurate interpretation of such measurements can provide direct information on the propagation and sources of CRs.

In the last few decades, progress has been made in detecting high-energy gamma-ray and neutrino emissions. The continuum diffuse gamma-ray emission has been well measured by the Fermi Large Area Telescope (LAT) up to a few hundred GeV [1,2]. Later, in the TeV energy regime, Milagro [3], ARGO-YBJ [4], H.E.S.S. [5–7], and HAWC [8,9] have contributed data regarding the Galactic plane. These measurements have only recently reached the PeV range thanks to the Tibet ASγ and LHAASO [10–12]. This discovery suggests the existence of PeVatrons [13], which are sources capable of accelerating particles up to PeV energies. This is a big step towards understanding cosmic-ray physics by exploring the knee region of the CR spectrum.

Since the first detection of astrophysical neutrinos in 2012, IceCube has been accumulating neutrino data for more than 10 years [14–16]. With the development of machine learning techniques and more statistics, the neutrino emission from the Galactic plane has recently been identified [17].

These achievements can provide a hint about the injection, distribution, and propagation of CRs in our Galaxy. However, the analysis of Galactic diffuse emission (GDE) can be contaminated by unresolved Galactic point sources which may have a distribution similar to the interstellar gas. Thus, it is a challenge to recognize the accelerator of CRs. Previously, a few groups have performed studies on the diffuse emission from TeV to PeV, where they discussed the possibility of the Galactic diffuse gamma-ray and neutrino emission coming from cosmic-ray interaction, known sources, and unresolved sources [18–22].

In this work, based on the current cosmic-ray and Fermi-LAT data, and the most recent LHAASO and IceCube Galactic plane observation, we apply the popular GALPROP

*linsj6@mail.sysu.edu.cn
†yanglli5@mail.sysu.edu.cn

code [23] to model CR transport and generate simulated spectra and maps of the diffuse gamma-ray and neutrino emissions. Specifically, we adopt a diffusion plus reacceleration (DR) model and employ DR-high and DR-low models to take into account the uncertainties of the measurements obtained from the ground-based air-shower experiments, IceTop and KASCADE, respectively. However, we find tension between the predicted gamma-ray flux with our constructed models and the observations. To illustrate the characteristic of the LHAASO Galactic plane spectrum and explain the excess, we create two populations of Galactic sources (EXTRA1 and EXTRA2) with exponential-cutoff-power-law (ECPL) spectra shape. In the energy range up to 10^5 GeV, the spectrum of EXTRA1 has an index of 2.40 and a cutoff energy of ~20 TeV. In the higher-energy range, up to 10^6 GeV, another component, EXTRA2, with an index of 2.3 and a cutoff of 2 PeV is introduced. This can be naturally explained by the two types of unresolved sources in our Galaxy with different maximum cosmic-ray energy.

Based on the constructed models, we also estimate the diffuse Galactic neutrino flux that is consistent with the latest IceCube Galactic plane search. We find that the Galactic neutrinos can contribute around 9% to the all-sky neutrino events at 20 TeV. At PeV energy, most of the neutrinos come from outside our Galaxy. However, due to a few uncertain factors—like the mechanisms, numbers, and distribution of these unresolved sources in our Galaxy and limited observation capabilities—there is still some space allowed for modeling. Therefore, to further reveal the problems, the next-generation Imaging Air Cherenkov Telescopes (IACTs) and neutrino detectors with a larger effective area and better angular and energy resolution, which can provide a precise location and morphology of sources, are in high demand.

The paper is organized as follows. Section II provides the description of the multimessenger data, including cosmic-ray, gamma-ray, and neutrino observations used in this work. In Sec. III, we present the injection and propagation models of cosmic rays, together with the addition of extra source components for fitting the gamma-ray data. Based on the constructed models, we show the calculated Galactic diffuse gamma-ray and neutrino emission in Sec. IV. In Sec. V, we give a discussion about the obtained results and the origins of the two extra components. In Sec. VI, we give a summary and future outlook for the multimessenger observations.

II. MULTIMESSENGER OBSERVATION

Thanks to the development of both satellites and ground-based observatories, diffuse high-energy neutrinos with energies between 10 TeV and PeV [24], ultra-high-energy cosmic rays (UHECRs, $> 10^{18}$ eV) [25], and high-energy gamma rays from MeV to PeV have been measured, or upper limits have been provided [8,12,26]. As there is a natural connection between these three messengers, neutrinos and gamma rays are produced during CR propagation and can directly point back to the origin of CRs. Their joint detection and analysis provide a very efficient way to explore the Universe [27,28]. Moreover, the energy budgets of UHECRs, PeV neutrinos, and isotropic sub-TeV gamma rays are comparable [29], which supports the unification of high-energy cosmic particles.

Before exploring, understanding, and identifying the mechanisms and physical processes of the astrophysical sources of CRs, the diffuse backgrounds originating from our Galaxy should be thoroughly studied. One accurate diffuse template can help analyze the upcoming data. For this purpose, we attempt to constrain the diffuse emission with current observations. The measurements used in this work are presented below.

A. High-energy cosmic rays

The high-energy CR particles are accelerated by energetic astrophysical sources like supernova remnants (SNRs), and they propagate inside the Galactic magnetic field around the Galactic disk after escaping. Although only the CR fluxes around the Sun could be measured, their distribution throughout the Galaxy can be predicted by the propagation model. Generally, the propagation model is constrained by the secondary-to-primary flux ratio observation, such as B/C [30] and ^{10}Be/^{9}Be [31]. More details regarding the propagation model can be found in Sec. III.

Their fluxes around the Earth have been directly measured by spaceborne experiments like AMS-02 [31–35] and the DArk Matter Particle Explorer (DAMPE) [30,36–38], and also indirectly measured by ground-based experiments like IceTop [39] and KASCADE [40].

Note that the measurements of the energies of the knees disagree between IceTop and KASCADE, as shown in Fig. 1. As the KASCADE experiment uses the QGSJET-II-02 model while IceTop uses the Sibyll 2.1 model, the discrepancies are caused by the large systematic uncertainty of the hadronic model. In our study, we refer to the models derived from KASCADE and IceTop data as DR-low and DR-high, respectively.

In this work, to estimate the diffuse gamma-ray and neutrino emission, the proton and electron plus positron spectra observed by Voyager, AMS-02, IceTop, and KASCADE are adopted to constrain the Galactic CR distribution, as seen in Figs. 1 and 2.

B. Gamma-ray sky

The diffuse gamma-ray emission has been well measured by a few satellites below TeV energies, such as EGRET, and followed by Fermi-LAT [26,41]. Recently, the Galactic plane has been observed up to 1 PeV, thanks to the Tibet ASγ and LHAASO [10,12] experiments. These discoveries show the evidence of hadronic origin of sub-PeV diffuse

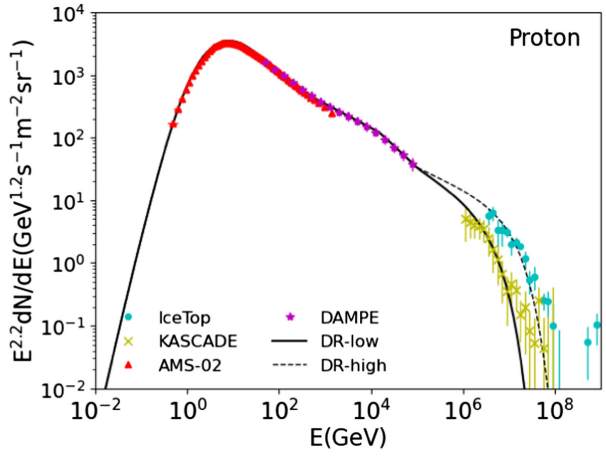

(a) proton

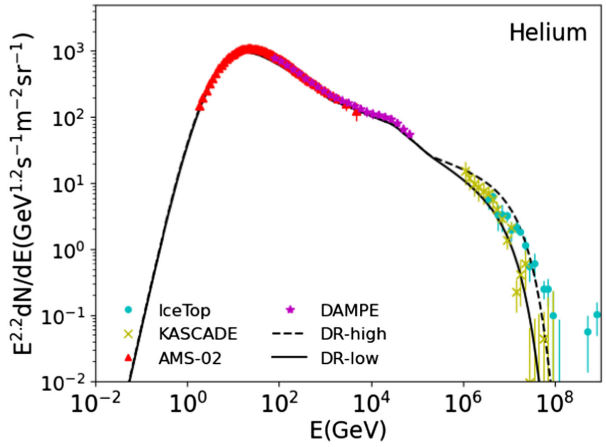

(b) helium

FIG. 1. Best-fitting spectra of protons (top) and helium nuclei (bottom), along with the observation data from IceTop (blue circles), KASCADE (yellow crosses), AMS-02 (red triangles), and DAMPE (purple stars). The solid line represents the DR-low model, while the dashed line represents the DR-high model.

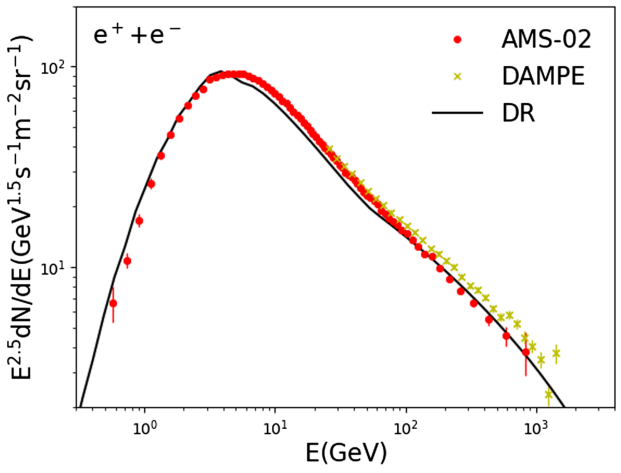

FIG. 2. Fitted electron plus positron spectrum (black solid line), and the measurements from AMS-02 (red dots) and DAMPE (yellow crosses).

gamma rays, which are generated during the propagation of tens of PeV CRs.

Recently, the LHAASO experiment announced the source-subtracted Galactic diffuse gamma-ray fluxes from the inner Galactic plane ($15° < l < 125°$, $|b| < 5°$) and outer plane ($125° < l < 235°$, $|b| < 5°$) for the first time. Here, a simple power law is adopted to describe the spectra for both regions with similar spectral indices of -2.99, which is consistent with the CR spectral index of the knee region.

In Fig. 3, the data for the window of $15° < l < 125°$, $|b| < 5°$ from the LHAASO and Fermi-LAT experiments [42], and for $25° < l < 100°$, $|b| < 5°$ from Tibet ASγ are presented. As can be seen, both the LHAASO and Tibet ASγ data are in agreement with the Fermi-LAT data. However, the result from LHAASO is a few times lower than that from ASγ. This is due to the different analysis methods of these two experiments. LHAASO analyzes the data by masking sources included in the TeVCAT with a radius of 5 times the Gaussian extension widths. Therefore, this cut procedure may lose a large part of the data of the Galactic plane, where the diffuse CR and unresolved sources are located.

C. Neutrino sky

Since the first observation of the astrophysical neutrino signal in the TeV–PeV energy range in 2012 [24], IceCube has continued to update the neutrino sky. The event distribution is consistent with being isotropic, and the origin of these neutrino signals is still unresolved. With larger statistics, IceCube has recently shown that there are more events at lower Galactic latitudes and a deficit of neutrino events at high Galactic latitudes [15]. The IceCube Neutrino Observatory has provided 6-year all-sky total and

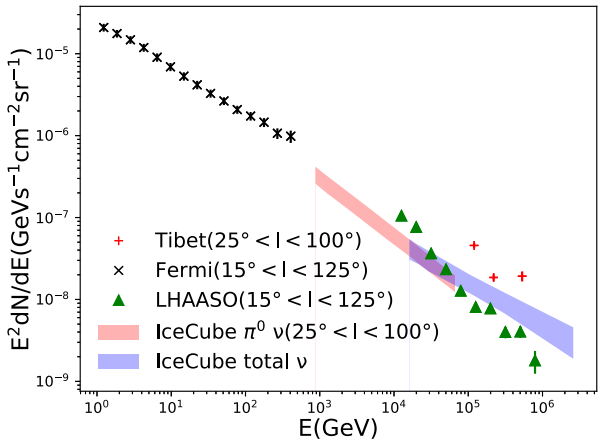

FIG. 3. Gamma-ray data from Fermi-LAT (black crosses) and LHAASO experiments (blue triangles) in the region of $15° < l < 125°$, $|b| < 5°$; gamma-ray data from Tibet ASγ (red plus), IceCube total ν (blue shaded region), and their results with the π^0 model in the Galactic plane (red shaded region).

10-year Galactic plane data [15,17]. In this recently updated data sample for the Galactic neutrino search, the analysis for the cascade events with lower energy thresholds was performed. The neutrino emission from the Galactic plane is reported at the 4.5σ level of significance [17], with a total of 59,592 events selected over the entire sky in the energy range of 500 GeV to several PeV. As shown in Fig. 3, the best-fitting Galactic plane neutrino flux is comparable with the gamma-ray flux.

The total neutrino observation, as shown by the blue shaded region in Fig. 3, includes events from Galactic and extragalactic diffuse backgrounds and astrophysical sources, whose spectrum follows a simple power-law distribution,

$$\Phi_\nu = \Phi_0 \left(\frac{E}{100\ \mathrm{TeV}} \right)^{-\gamma}. \quad (1)$$

Here, the normalization factor Φ_0 is $1.66 \times 10^{-18}\,\mathrm{GeV^{-1}\,cm^{-2}\,s^{-1}\,sr^{-1}}$, and the common spectral index γ is 2.53. The observed neutrino spectrum is softer than E^{-2}, which is comparable to the observed diffuse extragalactic gamma-ray background [43].

III. MODELS

Both the diffuse gamma-ray and neutrino flux are generated by CR particles when they propagate in the Galaxy. The hadronic component of CRs can induce gamma-ray and neutrino emission through proton-proton interactions, as well as bremsstrahlung radiation. On the other hand, the leptonic component of CRs contributes to gamma-ray emissions through the inverse Compton (IC) effect. To calculate these processes, along with the propagation effect of CRs, we utilize the well-established GALPROP code [23] in this study. In this section, we provide a detailed description of the CR propagation and emission model that are employed.

A. Cosmic-ray propagation

In the propagation model, CRs are assumed to undergo diffusion within the Galactic magnetic field, taking into account possible effects such as reacceleration, energy loss, fragmentation, and decay. The diffusion coefficient is parametrized as $D(R) = \beta^\eta D_0 (R/4\ \mathrm{GV})^\delta$, where D_0 is the normalization factor at a reference rigidity of 4 GV, R is the particle's rigidity, β is the velocity of the particles in natural units, δ is the slope of rigidity dependence, and η is a phenomenological parameter introduced to fit the low-energy secondary-to-primary ratios. Besides the diffusion, the convection or reacceleration effect is also required by the observed B/C data.

In some recent studies, with more secondary CR species like Li, Be, and B precisely measured by AMS-02, it was found that the reacceleration effect is favored [44]. In this work, we adopt a DR model as a benchmark. The model parameters that describe the propagation processes are adopted following the work of other groups [44], corresponding to the best-fit values obtained by fitting the Li, Be, B, C, and O measurements from AMS-02. As listed in Table I, the half height of diffuse zone z_h is 6.3 kpc, and the Alfven speed v_A that describes the strength of reacceleration is 33.76 $\mathrm{km\,s^{-1}}$.

TABLE I. Propagation parameters.

D_0	δ (10^{28} $\mathrm{cm^2\,s^{-1}}$)	z_h (kpc)	v_A ($\mathrm{km\,s^{-1}}$)	η
7.69	0.362	6.3	33.76	−0.05

B. Cosmic-ray injection

It is widely accepted that SNRs are the most promising Galactic high-energy CR sources, whose shock provides the ideal environment for first-order Fermi accelerations of relativistic particles. Of the 12 Galactic PeV accelerators discovered by LHAASO, eight are somehow linked to SNRs [11]. Therefore, we make a simple assumption that CRs are injected into the Galaxy by the SNRs. As it is not possible to gather information on all historical SNRs, for an estimation, we employ a continuous source distribution for SNRs as follows:

$$f(r,z) = \left(\frac{r}{r_\odot} \right)^{1.25} \exp\left[-\frac{3.56(r-r_\odot)}{r_\odot} \right] \exp\left(-\frac{|z|}{z_s} \right), \quad (2)$$

where $r_\odot = 8.3$ kpc is the distance from the Sun and $z_s = 0.2$ kpc is a scale factor that indicates the thickness of the Galactic disk.

Given the many spectral structures revealed by recent direct detection experiments, the injection spectra of CRs may be quite complicated. A multiple-broken-power-law spectrum is employed to describe these features:

$$f(x) = \begin{cases} R^{-\nu_0} e^{-\frac{R}{Rc}} & R < R_1 \\ \left(\prod_{i=1}^{n} R_i^{\nu_i - \nu_{i-1}} \right) R^{-\nu_n} e^{-\frac{R}{Rc}} & R_n \le R < R_{n+1} \\ \left(\prod_{i=1}^{4} R_i^{\nu_i - \nu_{i-1}} \right) R^{-\nu_4} e^{-\frac{R}{Rc}} & R_4 \le R, \end{cases} \quad (3)$$

where n in the second row is from 1 to 3. The corresponding observation could constrain the injection parameters in Eq. (3) for different CR species. As there exist discrepancies between the IceTop and KASCADE measurements, we construct two models, differing in their injections, to indicate the upper and lower boundaries of theoretical estimation, so-called DR-high and DR-low models, respectively.

Following Ref. [42], the spectral structures are assumed to be mainly due to the source injection as in Eq. (3), without taking into account the change of propagation

TABLE II. Source injection and solar modulation parameters as in Eq. (3) for the proton and helium nuclei.

	Proton		Helium	
	DR-high (IceTop)	DR-low (KASCADE)	DR-high (IceTop)	DR-low (KASCADE)
ν_0	2.06	2.06	1.46	1.46
ν_1	2.43	2.43	2.36	2.36
ν_2	2.22	2.22	2.12	2.12
ν_3	2.52	2.52	2.42	2.42
ν_4	2.18	2.32	2.08	2.28
R_1/GV	13.9	13.9	1.99	1.99
R_2/TV	0.50	0.50	0.65	0.65
R_3/TV	15.0	15.0	15.0	15.0
R_4/TV	100.0	100.0	100.0	100.0
R_c/PV	12.0	4.0	6.0	4.0
Φ/GV	0.700	0.700	0.700	0.700

parameters. The constraints for the proton, helium, and electron plus positron are performed. These three kinds of CR particles play a major role in contributing to Galactic γ and neutrino emission. We develop our neutrino and gamma-ray sky map based on these best-fitting parameters, listed in Tables II and III. The comparisons between observation and the model are shown in Figs. 1 and 2.

As seen in Table II, for both the DR-high and DR-low models, most of the best-fitting parameters ν_i and R_i are identical to each other, except R_c and ν_4. Here, R_c represents the characteristic cutoff rigidity of the exponential cutoff spectrum, describing the knee energy of those particles. Apparently, the R_c of the DR-high model is higher than that of the DR-low model because of the different knee energies from IceTop and KASCADE. On the other hand, the ν_4 of the DR-high model is smaller than that of the DR-low model, which is due to a harder spectrum from the IceTop measurement.

C. Gamma-ray expectation

With the propagation and injection of CRs fixed, we analyze the gamma-ray sky map. We apply the GALPROP code to calculate the diffuse emissions from a few processes, including natural pion decay, bremsstrahlung, and inverse Compton scattering (ICS). The AAfrag package [45] is adopted to estimate the secondary gamma-ray and neutrino production from inelastic hadronic interactions.

We show the diffuse gamma-ray spectra measured by the LHAASO and Fermi-LAT experiments, along with our model predictions for both the inner region [Figs. 4(a) and 4(c)] and the outer region [Figs. 4(b) and 4(d)]. To ensure a self-consistent comparison, we apply the same masks as in the LHAASO analysis [12] for all calculated results and data.

Compared with the gamma-ray data from Fermi-LAT and LHAASO, the predicted flux with the DR-high-only model is consistent with the data at energies less than a few GeV as well as above 60 TeV. However, between a few GeV and 60 TeV, the DR-high-only model cannot explain the LHAASO data, as can be seen in Figs. 4(c) and 4(d).

This excess below 60 TeV was initially identified through the analysis of GeV Fermi-LAT observations [1]. To account for this excess, some studies have proposed a spatially dependent diffusion model [46]. However, this modification of the propagation model is insufficient to explain the data obtained by LHAASO.

In this work, we attribute this TeV excess to unresolved sources along the Galactic plane, which are expected to be numerous and faint within the field of view of LHAASO and Fermi-LAT. Various physical interpretations have previously been discussed in the literature [47–49]. Among these interpretations, the pulsar TeV halo and pulsar wind nebulae (PWNe) have emerged as potential candidates [48,49]. Therefore, to fit the bump $\sim\mathcal{O}(1)$ TeV in the LHAASO spectrum, we employ an ECPL component (named EXTRA1) with an index of 2.4 and a cutoff of 20 TeV to describe these unresolved sources that follow the spatial distribution of pulsars.

The cutoff energy of the introduced EXTRA1 in this work is lower than that of the extra component in Ref. [42] (30 TeV), as we have introduced the EXTRA2 to account for the high-energy data.

However, this component is insufficient for the DR-low case, where an additional component is required at PeV energy. Therefore, another ECPL component (EXTRA2) with an index of 2.3 and a cutoff at 2 PeV is introduced for the DR-low case. These EXTRA1 and EXTRA2 components have close spectral indices, around the average spectral index of sources in the H.E.S.S. Galactic Plane Survey, but different cutoff energies. The cutoff energies of gamma rays for different scenarios indicate different maximum energies of CR particles. For instance, for the leptonic (hadronic) origin, the 20-TeV gamma-ray cutoff energy corresponds to 700 TeV (100 TeV) electron/positron (proton)

TABLE III. Source injection and solar modulation parameters of the electron plus positron.

ν_0^-	ν_1^-	ν_2^-	ν_3^-	R_1^-/GV	R_2^-/GV	R_3^-/GV	R_c^-/TV	Φ^-/GV
2.33	0.01	2.88	2.45	0.950	4.19	55.7	6.27	1.1
c_{e^+}	ν_1^+	ν_2^+	R_1^+/GV	R_c^+/TV	Φ^+/GV			
1.00	3.04	2.08	31.2	3.42	1.1			

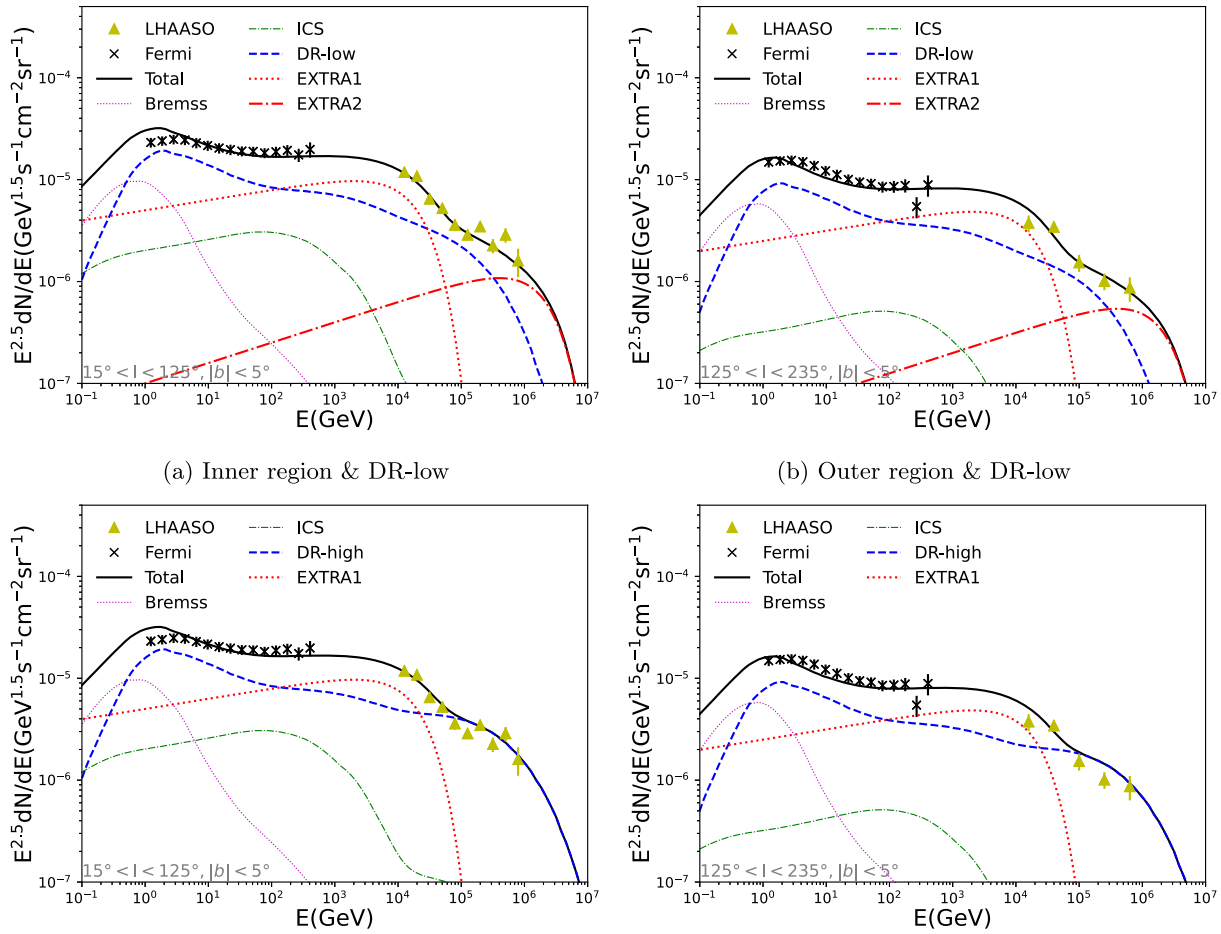

(a) Inner region & DR-low

(b) Outer region & DR-low

(c) Inner region & DR-high

(d) Outer region & DR-high

FIG. 4. Diffuse gamma-ray emission calculated from the DR model. The physical radiation of ICS (green dot-dashed line), bremsstrahlung (pink dotted line), and pion decay (blue dashed line) is shown. Two extra source components, EXTRA1 (red dotted line) and EXTRA2 (red dot-dashed line) with ECPL spectra, are presented. Panels (a) and (b) are the spectra obtained from the DR-low model, and panels (c) and (d) are for the DR-high model. Panels (a) and (c) show the results for the inner Galaxy region of $15° < l < 125°$, $|b| < 5°$, while panels (b) and (d) display the results for the outer Galaxy region of $125° < l < 235°$, $|b| < 5°$.

cutoff energy. This suggests that EXTRA1 and EXTRA2 likely represent at least two distinct types of unresolved sources in the Galaxy.

Recent studies indicate that this excess, such as our EXTRA1 components, is usually of leptonic origin, as strongly constrained by the hardening of the local cosmic-ray proton spectrum observed by AMS. However, no source class has been uncovered.

For EXTRA2 sources contributing at higher energies, there is no constraint from current cosmic-ray observations. If they are of leptonic origin, such as PWNe, the Klein-Nishina regime is dominant. Therefore, a very high acceleration rate is required, and it should also be higher than the electron radiative losses. This is quite stringent. If EXTRA2 sources are TeV halos, some studies argued that a slower diffusion of the electrons in the interstellar medium is needed [50], which is still not understood. Therefore, the hadronic model cannot be excluded. To confirm and deeply explore the source mechanisms of both EXTRA1 and EXTRA2, neutrino signals would provide direct evidence for this mystery.

IV. RESULTS

A. Galactic diffuse gamma-ray emission

Based on the constructed model, we generate a diffuse gamma-ray emission map which can be used as a template for future studies. This map consists of four components: ICS, bremsstrahlung, natural pion decay, and extra source contributions. Except for bremsstrahlung and neutral pion decay, the spatial distributions of all these components are different from each other. In Fig. 5, we show the gamma-ray energy spectrum for the region of $25° < l < 100°$, $|b| < 5°$ without masking as an example. In general, this spectrum is higher than that of the region $15° < l < 125°$, which might be due to the masking effect

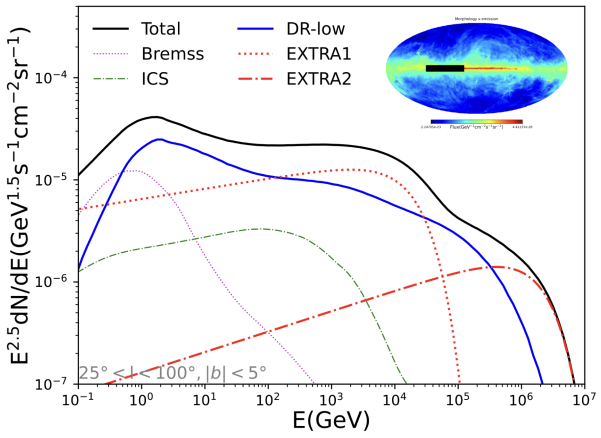

FIG. 5. Diffuse gamma-ray emission calculated from the DR-low model. The physical radiation of ICS (green dot-dashed line), bremsstrahlung (pink dotted line), and pion decay (blue dashed line) is shown. Two extra source components, EXTRA1 (red dotted line) and EXTRA2 (red dot-dashed line) with ECPL spectra, are presented. This figure shows the result for the inner Galaxy region of $25° < l < 100°$, $|b| < 5°$.

from the LHAASO analysis. For any other region of interest, the predicted gamma-ray emission can be selected in the same manner to serve as a background template for point source analysis.

B. Galactic diffuse neutrino

We show the neutrino sky map from 100 TeV to 10 PeV from Sec. III in Fig. 6. As one can see in Figs. 7(a) and 7(b), our prediction for Galactic diffuse neutrino emission for both the all-sky and Galactic plane with the DR-low model are in agreement with IceCube best-fitting flux normalizations from the data [17]. However, for the π^0 template of IceCube, an extra source contribution with a hadronic origin is needed. This appears to contradict the fact that these sources only contribute to gamma-ray emissions and not cosmic rays.

For comparison, IceCube's total neutrino is also shown here. Our calculated Galactic diffuse neutrino flux shows

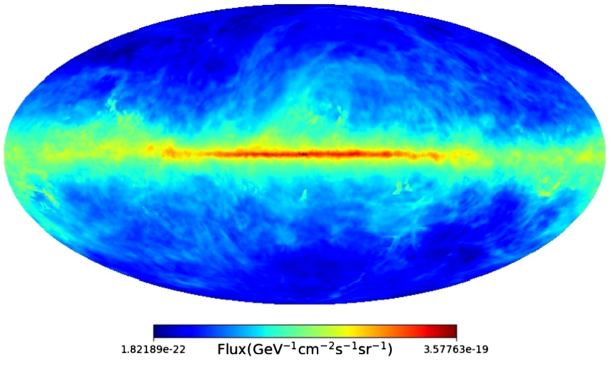

FIG. 6. Calculated Galactic diffuse neutrino map with energies from 100 TeV to 10 PeV. The morphology follows the gas distribution in our Galaxy.

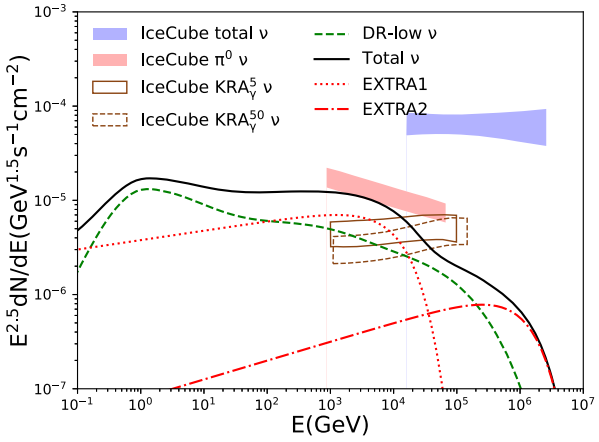

(a) all-sky

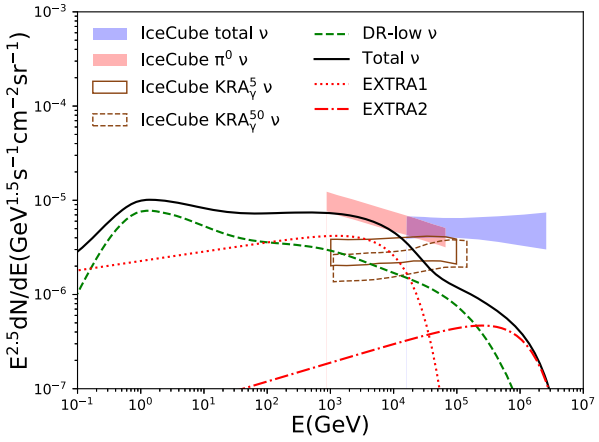

(b) $25° < l < 100°$, $|b| < 5°$

FIG. 7. Predicted neutrino flux per flavor from the DR-low model compared with the IceCube total data (blue shaded region), their π^0 model (red shaded region), the KRA_γ^5 model (region with the brown solid edge), and the KRA_γ^{50} model (region with the brown dashed edge). Other components—including EXTRA1 (red dotted line), EXTRA2 (red dot-dashed line), neutrino flux with the DR-low model (green dashed line), and total ν flux (black solid line)—are shown. Panel (a) is for the all-sky region, and panel (b) is the region of $25° < l < 100°$, $|b| < 5°$.

that the contribution of Galactic neutrinos to the total neutrino observation is around 9% at 20 TeV, as seen in Fig. 7(a).

In Fig. 7(b), we present a comparison of the surface brightness of one flavor neutrino between the Galactic contribution in the disk region ($|b| < 5°$, $25° < l < 100°$) and the total contribution averaged over the all-sky region. This shows the distinctiveness of the neutrino Galactic disk compared to the isotropic neutrino background. The neutrino flux of the Galactic disk is prominent in the energy range from 10 TeV to 100 TeV and decreases significantly at higher energies. This is constrained by the gamma-ray and cosmic-ray measurements. Our results are in agreement with other studies [17,51]. The Milky Way is

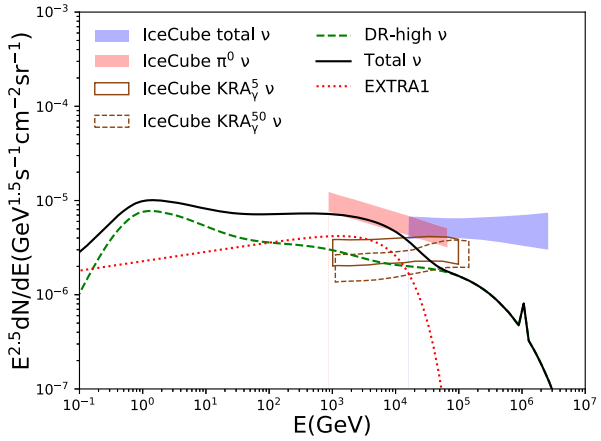

FIG. 8. Predicted neutrino flux per flavor for the DR-high model compared with the IceCube total data (blue shaded region), their π^0 model (red shaded region), the KRA$_\gamma^5$ model (region with the brown solid edge), and the KRA$_\gamma^{50}$ model (region with the brown dashed edge). The neutrino flux from EXTRA1 (red dotted line), the DR-high model (green dashed line), and total ν flux (black solid line) are shown for the region of $25° < l < 100°$, $|b| < 5°$.

a source of high-energy neutrinos consistent with the gamma-ray observation, as seen in Figs. 7(a) and 5.

In the case of the DR-high-only model, as seen in Fig. 8, the calculated neutrino flux is consistent with two best-fitting results with the KRA$_\gamma$ model. At a few PeV, the Glashow resonance is shown in the spectrum [52]. However, to explain the results for the π^0 model, EXTRA1 would be necessary.

V. DISCUSSION

In this work, based on the most recent PeV Galactic diffuse gamma-ray observation from LHAASO, with two sets of CR data from IceTop and KASCADE, we construct our DR-high and DR-low models separately. For both models, we find it is hard to explain the LHAASO Galactic plane search with conventional CR propagation. After adding extra source contributions, the diffuse gamma-ray emission can be well explained by both the DR-high model with EXTRA1 (Model 1) and the DR-low model with both EXTRA1 and EXTRA2 (Model 2).

For Model 1, one extra source spectrum EXTRA1 is introduced, with a spectral index of 2.4 and a cutoff of 20 TeV. For Model 2, two extra source contributions are introduced—one with an index of 2.4 and a cutoff energy of 20 TeV and another with an index of 2.3 and a cutoff energy of 2 PeV. Thus, there could be two populations of sources in our Galaxy, with faint gamma-ray emission which is lower than the sensitivity of our current instruments, so they have not been identified. They follow similar CR accelerated mechanisms with a close spectral index but various maximum CR energy.

Based on the obtained model, we simulate the Galactic diffuse neutrino flux, obtaining the sky map as shown in Fig. 6. For example, with Model 2, we estimate the Galactic contribution of the astrophysical flux is around 9% at 20 TeV. It is uncertain if these Galactic neutrinos are from the CR propagation or point sources because of insufficient statistical power. Therefore, we believe the future Imaging Air Cherenkov Telescope [53] and the upgraded neutrino observatory will resolve the point sources, precisely provide the diffuse map, and reveal the origin and propagation of cosmic rays.

The best-fitting Galactic neutrino flux from IceCube is model dependent. Here, the π^0 model is constrained by the Fermi MeV to GeV gamma-ray emission and is extrapolated to TeV, where the same spatial emission profile is assumed. However, KRA$_\gamma$ models take into account the spatial distribution of spectra, and cutoff energies of 5 and 50 PeV, respectively. Therefore, the π^0 model provides an even event distribution along the Galactic plane, and KRA$_\gamma$ models give a higher neutrino flux at the Galactic center region. Thus, for the region of interest, $25° < l < 100°$, $|b| < 5°$, the π^0 model gives a higher flux than that from KRA$_\gamma$ models. On the other hand, the cosmic-ray diffuse modeling with GALPROP for the DR-low and DR-high models in this work is not consistent with the KRA models from the Dragon analysis. The discrepancy between all these models is due to the low statistics and the uncertainty of the current templates. Further accurate measurements and studies are quite essential. We summarize the differences in Table IV.

With only the gamma-ray and cosmic-ray observations, EXTRA1 sources prefer to be of leptonic origin, which has been discussed by a few groups. However, in the case of IceCube's best-fitting flux for the π^0 model, which is the only one consistent with the recent observations of 100-TeV gamma rays by the Tibet ASγ [10], a population of EXTRA1 sources with a hadronic scenario would be necessary in both the DR-high and DR-low models, as seen in Figs. 7 and 8. This kind of source would be required to inject fewer high-energy protons. Thus, the identification of neutrinos can reveal the origin of CRs, modify the CR propagation and distribution models drastically, and explore the history of our Galaxy. This can occur if EXTRA1 sources are of leptonic origin, where no neutrino is produced. A tension exists between the predicted diffuse Galactic neutrino flux and the IceCube results for the π^0 model.

IceCube's best-fitting fluxes for the KRA$_\gamma$ models provide the lower limit for the neutrino emission from

TABLE IV. Scenario in which the extra source meets the measurements of cosmic rays, gamma rays, and neutrinos.

Origin	p	ν	γ
Leptonic	✓	KRA$_\gamma$	✓
Hadronic	Hadronless	π^0	✓

the Galactic plane. No other extra hadronic sources are needed. In other words, the EXTRA1 sources would be of leptonic origin. Thus, no extra proton injection is needed, and the tension is released between the data and models.

No matter which results are used for the different model templates obtained by IceCube, both the leptonic and hadronic origins of the EXTRA2 source are allowed by data. High-energy neutrino emission is a unique diagnostic for hadronic content. Using future PeV neutrino detection with improved sensitivity, the EXTRA2 sources could be identified. If EXTRA2 of Model 2 is of hadronic origin, the Galactic neutrino will contribute around 1% to the total IceCube neutrino at PeV. Otherwise, the contribution is ∼0.4%.

VI. SUMMARY

In summary, thanks to the recent observations by LHAASO [12] and IceCube [17], the Galactic diffuse sky has become richer, especially in the high-energy regime. The LHAASO measurements show a bump in the gamma-ray spectrum, where contributions from extra unresolved sources are needed. The IceCube Collaboration confirmed the high-energy neutrinos from the Galactic plane. Our calculated flux with models obtained from gamma-ray observations is consistent with the neutrino data. However, for the best-fitting results for the π^0 model from IceCube data, the EXTRA1 sources in the hadronic scenario are necessary to fill the gap between the calculated flux and data, even though this would be disfavored by CR measurements.

The joint analysis of cosmic rays, gamma rays, and neutrinos has proven to be capable of understanding the high-energy sky. For example, the diffuse gamma-ray detection by LHAASO can probe the CR density in our Galaxy and solve the problem of the disagreement between IceTop and KASCADE. In addition, the neutrino detection can reveal hidden sources that are not transparent for gamma-ray emission.

The current results from all three messengers are in agreement with each other. More evidence shows the existence of PeVatrons in our Galaxy. The next step should be to identify the mysterious astronomical origin of high-energy cosmic rays with upgraded neutrino and gamma-ray detectors.

ACKNOWLEDGMENTS

We thank the referees for helpful comments and suggestions. This work is supported by the National Natural Science Foundation of China (NSFC) Grants No. 12005313, No. 12205388, and No. 12261141691.

[1] M. Ackermann, M. Ajello, W. Atwood, L. Baldini, J. Ballet, G. Barbiellini, D. Bastieri, K. Bechtol, R. Bellazzini, B. Berenji *et al.*, Astrophys. J. **750**, 3 (2012).
[2] M. Ackermann, M. Ajello, A. Albert, W. Atwood, L. Baldini, J. Ballet, G. Barbiellini, D. Bastieri, K. Bechtol, R. Bellazzini *et al.*, Astrophys. J. **799**, 86 (2015).
[3] A. A. Abdo *et al.*, Astrophys. J. **688**, 1078 (2008).
[4] B. Bartoli *et al.* (ARGO-YBJ Collaboration), Astrophys. J. **806**, 20 (2015).
[5] F. Aharonian, A. Akhperjanian, U. B. De Almeida, A. Bazer-Bachi, Y. Becherini, B. Behera, W. Benbow, K. Bernlöhr, C. Boisson, A. Bochow *et al.*, Phys. Rev. Lett. **101**, 261104 (2008).
[6] H. Abdalla *et al.* (HESS Collaboration), Astron. Astrophys. **612**, A9 (2018).
[7] H. Abdalla, A. Abramowski, F. Aharonian, F. A. Benkhali, E. Angüner, M. Arakawa, M. Arrieta, P. Aubert, M. Backes, A. Balzer *et al.*, Astron. Astrophys. **612**, A1 (2018).
[8] A. Aab, P. Abreu, M. Aglietta, I. Albuquerque, J. M. Albury, I. Allekotte, A. Almela, J. A. Castillo, J. Alvarez-Muñiz, G. A. Anastasi *et al.*, J. Cosmol. Astropart. Phys. (2019) 022.
[9] A. Albert, R. Alfaro, C. Alvarez, J. A. Camacho, J. Arteaga-Velázquez, K. Arunbabu, D. A. Rojas, H. A. Solares, V. Baghmanyan, E. Belmont-Moreno *et al.*, Astrophys. J. **905**, 76 (2020).
[10] M. Amenomori *et al.* (Tibet ASgamma Collaboration), Phys. Rev. Lett. **126**, 141101 (2021).
[11] Z. Cao *et al.* (LHAASO Collaboration), Nature (London) **594**, 33 (2021).
[12] Z. Cao *et al.* (LHAASO Collaboration), arXiv:2305.05372.
[13] T. Sudoh and J. F. Beacom, Phys. Rev. D **107**, 043002 (2023).
[14] M. G. Aartsen *et al.* (IceCube Collaboration), Astrophys. J. **849**, 67 (2017).
[15] M. G. Aartsen *et al.* (IceCube Collaboration), Astrophys. J. **886**, 12 (2019).
[16] A. Albert *et al.* (ANTARES and IceCube Collaborations), Astrophys. J. Lett. **868**, L20 (2018).
[17] R. Abbasi *et al.* (IceCube Collaboration), Science **380**, adc9818 (2023).
[18] P. D. l. T. Luque, D. Gaggero, D. Grasso, O. Fornieri, K. Egberts, C. Steppa, and C. Evoli, Astron. Astrophys. **672**, A58 (2023).
[19] K. Egberts, C. Steppa, and K. P. Peters, *Proc. Sci.*, Gamma2022 (2023) 230 [arXiv:2303.11850].
[20] P. De La Torre Luque, D. Gaggero, and D. Grasso, *Proc. Sci.* ECRS2023 (2023) 103.
[21] G. Schwefer, P. Mertsch, and C. Wiebusch, Astrophys. J. **949**, 16 (2023).

[22] S. Gabici, C. Evoli, D. Gaggero, P. Lipari, P. Mertsch, E. Orlando, A. Strong, and A. Vittino, Int. J. Mod. Phys. D **28**, 1930022 (2019).
[23] A. W. Strong and I. V. Moskalenko, Astrophys. J. **509**, 212 (1998).
[24] M. G. Aartsen *et al.* (IceCube Collaboration), Science **342**, 1242856 (2013).
[25] The Pierre Auger Observatory: Contributions to the 34th International Cosmic Ray Conference (ICRC 2015) (2015), arXiv:1509.03732.
[26] W. B. Atwood *et al.* (Fermi-LAT Collaboration), Astrophys. J. **697**, 1071 (2009).
[27] M. G. Aartsen *et al.* (IceCube, Fermi-LAT, MAGIC, AGILE, ASAS-SN, HAWC, H.E.S.S., INTEGRAL, Kanata, Kiso, Kapteyn, Liverpool Telescope, Subaru, Swift NuSTAR, VERITAS, and VLA/17B-403 Collaborations), Science **361**, eaat1378 (2018).
[28] B. P. Abbott *et al.* (LIGO Scientific, Virgo, Fermi-GBM, and INTEGRAL Collaborations), Astrophys. J. Lett. **848**, L13 (2017).
[29] K. Fang and K. Murase, Nat. Phys. **14**, 396 (2018).
[30] D. Collaboration, Sci. Bull. **67**, 2162 (2022).
[31] M. Aguilar *et al.* (AMS Collaboration), Phys. Rev. Lett. **117**, 231102 (2016).
[32] M. Aguilar *et al.* (AMS Collaboration), Phys. Rev. Lett. **114**, 171103 (2015).
[33] M. Aguilar *et al.* (AMS Collaboration), Phys. Rev. Lett. **119**, 251101 (2017).
[34] M. Aguilar *et al.* (AMS Collaboration), Phys. Rev. Lett. **122**, 101101 (2019).
[35] M. Aguilar *et al.* (AMS Collaboration), Phys. Rev. Lett. **122**, 041102 (2019).
[36] F. Alemanno *et al.*, Phys. Rev. Lett. **126**, 201102 (2021).
[37] Q. An, R. Asfandiyarov, P. Azzarello, P. Bernardini, X. J. Bi, M. S. Cai, J. Chang, D. Y. Chen, H. F. Chen, J. L. Chen *et al.*, Sci. Adv. **5**, eaax3793 (2019).
[38] G. Ambrosi, Q. An, R. Asfandiyarov, P. Azzarello, P. Bernardini, B. Bertucci, M. S. Cai, J. Chang, D. Y. Chen, H. F. Chen *et al.*, Nature (London) **552**, 63 (2017).
[39] M. G. Aartsen *et al.* (IceCube Collaboration), Phys. Rev. D **100**, 082002 (2019).
[40] T. Antoni *et al.* (KASCADE Collaboration), Astropart. Phys. **24**, 1 (2005).
[41] S. D. Hunter *et al.*, Astrophys. J. **481**, 205 (1997).
[42] R. Zhang, X. Huang, Z.-H. Xu, S. Zhao, and Q. Yuan, arXiv:2305.06948.
[43] K. Bechtol, M. Ahlers, M. Di Mauro, M. Ajello, and J. Vandenbroucke, Astrophys. J. **836**, 47 (2017).
[44] Q. Yuan, C.-R. Zhu, X.-J. Bi, and D.-M. Wei, J. Cosmol. Astropart. Phys. 11 (2020) 027.
[45] M. Kachelrieß, I. V. Moskalenko, and S. Ostapchenko, Comput. Phys. Commun. **245**, 106846 (2019).
[46] Y.-Q. Guo and Q. Yuan, Phys. Rev. D **97**, 063008 (2018).
[47] D. Kantzas, S. Markoff, A. J. Cooper, D. Gaggero, M. Petropoulou, and P. D. L. T. Luque, Mon. Not. R. Astron. Soc. **524**, 1326 (2023).
[48] T. Linden and B. J. Buckman, Phys. Rev. Lett. **120**, 121101 (2018).
[49] V. Vecchiotti, F. Zuccarini, F. L. Villante, and G. Pagliaroli, Astrophys. J. **928**, 19 (2022).
[50] F. Aharonian, Q. An, Axikegu, L. X. Bai, Y. X. Bai, Y. W. Bao, D. Bastieri, X. J. Bi, Y. J. Bi, H. Cai *et al.* (LHAASO Collaboration), Phys. Rev. Lett. **126**, 241103 (2021).
[51] Y. Y. Kovalev, A. V. Plavin, and S. V. Troitsky, Astrophys. J. Lett. **940**, L41 (2022).
[52] S. L. Glashow, Phys. Rev. **118**, 316 (1960).
[53] P. D. Marinos, G. P. Rowell, T. A. Porter, and G. Jóhannesson, Mon. Not. R. Astron. Soc. **518**, 5036 (2022).